Hindawi Publishing Corporation
Journal of Nanomaterials
Volume 2014, Article ID 212637, 17 pages
http://dx.doi.org/10.1155/2014/212637

Review Article

Transmissive/Reflective Structural Color Filters: Theory and Applications

Yan Yu,[1,2] Long Wen,[2] Shichao Song,[2] and Qin Chen[2,3]

[1] *Department of Physics, Shanghai University, Shanghai 200444, China*
[2] *Key Lab of Nanodevices and Applications-CAS and Collaborative Innovation Center of Suzhou Nano Science and Technology, Suzhou Institute of Nano-Tech and Nano-Bionics, Chinese Academy of Sciences (CAS), Suzhou 215123, China*
[3] *Peking University Shenzhen SOC Key Laboratory, PKU-HKUST Shenzhen-Hong Kong Institute, Hi-Tech Industrial Park South, Shenzhen 518057, China*

Correspondence should be addressed to Qin Chen; qchen2012@sinano.ac.cn

Received 28 February 2014; Accepted 18 April 2014; Published 15 July 2014

Academic Editor: Tong Zhang

Structural color filters, which obtain color selection by varying structures, have attracted extensive research interest in recent years due to the advantages of compactness, stability, multifunctions, and so on. In general, the mechanisms of structural colors are based on the interaction between light and structures, including light diffraction, cavity resonance, and surface plasmon resonance. This paper reviews recent progress of various structural color techniques and the integration applications of structural color filters in CMOS image sensors, solar cells, and display.

1. Introduction

Color is one of the most important properties of vision. The color filters, either reflective or transmissive, provide the ability to select individual colors from a white light, which is the prerequisite of colorful imaging and display. Pigment and dye are the most popularly used color filters, which are based on the material selective absorption in the visible band [1]. Various pigments or dyes have to be integrated together by multistep processing to realize a colorful image. For example, in an image sensor with pixels arranged in Bayer's array, three aligned photolithography processes are necessary to define the red, green, and blue color pixels [2]. Alternatively, color can be generated by manipulating the propagation of light, for example, using dispersive gratings based on the light diffraction theory. It can be found in nature like the wings of butterflies [3, 4], where different structures on the wings show different colors. In contrast to the pigments and dyes, the called *structural color* is based on the interaction between light and the structures rather than the material properties. As a result, a complete set of structural color filters can be readily achieved in the same material by single-step patterning of different structures, which provides structural color with a great chance to gain high compactness and cut down the cost. Furthermore, structural color has high resistance to the chemicals and high stability to the heat and radiation and therefore can be used in the extreme environment like the aerospace.

In this review, we will discuss the mechanisms of various structural color filtering techniques for both reflective and transmissive color filters and then focus on the integrated applications of structural color in the fields of imaging, display, and colorful solar cells. Finally, we will summarize the current issues of structural color and possible resolutions.

2. Transmissive/Reflective Structural Color Filters

2.1. Metallic Nanohole Array Color Filters. As is well known, light is usually blocked by a metal sheet and therefore metallic coatings are widely used as mirrors. In 1998, Ebbesen et al. observed the extraordinary optical transmission (EOT) through a sliver film with periodic subwavelength

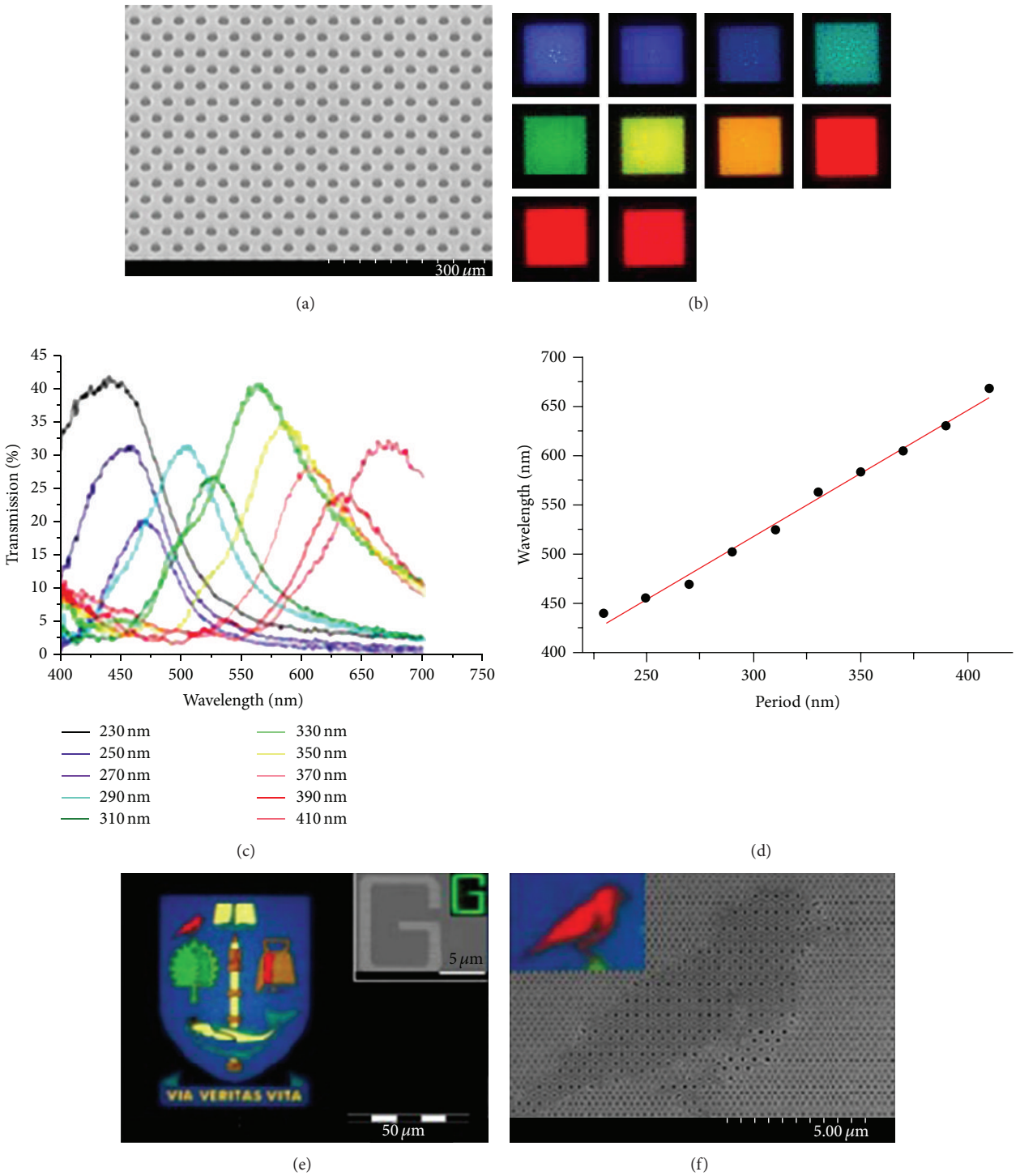

FIGURE 1: Metallic circular hole array transmissive color filters. (a) A SEM image of a hole array in aluminum at a period of 410 nm. (b) Images of hole arrays in different periods taken in microscope transmission mode under a white light illumination. (c) Transmissive spectra of the arrays shown in (b). (d) Wavelengths at the transmission peaks versus the period [17]. (e) Full-color images in microscope transmission mode. Inset is a patterned letter "G" with a 1-μm-wide line showing green color. (f) SEM image of a section of the fabricated logo pattern. The inset is the enlarged microscope image [18].

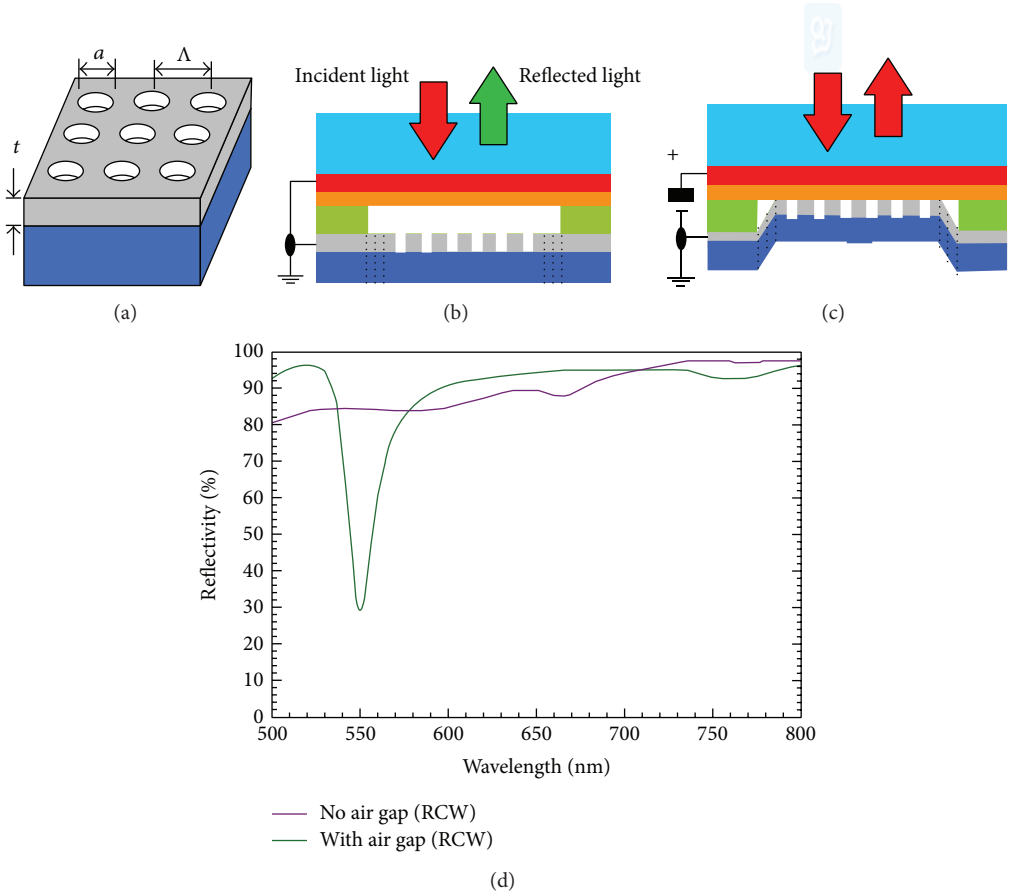

FIGURE 2: Tunable color filter. (a) Schematic of a nanohole array on SOI. (b) The nanohole array has an air gap from the glass plate, that is, "OFF" state. (c) The nanohole array contacts the glass plate, that is, "ON" state. (d) The reflective spectra [27].

hole arrays [5], which contradicts Bethe's theory on light diffraction by small holes [6]. Although there are debates on the physical mechanisms of this EOT effect, most researchers agree that surface plasmonic resonance (SPR) plays an important role in the color filtering [7–10]. To excite SPR, periodic gratings are usually used to match the wavevector of incident light and that of SPR. The resonant wavelength λ_0, that is, the transmission peak, is mainly determined by the pattern geometry [11]

$$\lambda_0 = \left(2\pi\sqrt{\frac{\varepsilon_m\varepsilon_d}{\varepsilon_m+\varepsilon_d}}\right) \times \left(\left(k_{\parallel}\cos\phi + i\frac{2\pi}{a_x} + j\frac{2\pi}{a_x}\right)^2 + \left(k_{\parallel}\sin\phi - i\frac{2\pi}{a_y} + j\frac{2\pi}{a_y}\right)^2\right)^{-1/2}, \quad (1)$$

where $k_{\parallel}$ is the in-plane wave vector magnitude, ϕ is the azimuthal angle of incident light, a_x and a_y are the lattice dimensions, i and j are the scattering orders of the array, and ε_m and ε_d are the permittivity for the metal and dielectric medium. As shown, the transmissive color can be tuned by simply changing the periods for given material parameters. Metallic hole array color filters in triangular lattice [12–18] and square lattice [19–21] with circular hole [12, 14–21], triangular hole [13], square hole [22], and annular hole [16] have been reported both theoretically and experimentally. Genetic algorithm was used to design filters with the spectral spectrum matching the 1931 International Commission on Illumination color matching functions [8]. Electron beam lithography (EBL) [11–13], nanoimprint [20, 23–25], and nanotransfer print [26] were used to pattern the nanohole array. Chen, one of the authors, fabricated circular hole arrays in triangular lattices in a 150 nm aluminum film [11, 17, 18]. The experimental results are shown in Figure 1. Very regular holes were patterned by EBL in a region of $50 \times 50\ \mu m^2$ for each color. The spectral response was characterized using a microscope spectrometer. The wavelength of transmission peak is found to be nearly linear to the period as shown in Figure 1(d). The transmission is approximately 30% and the full width at half maximum (FWHM) is less than 100 nm. To demonstrate the full control of the color and the high resolution, a complex colorful pattern consisting of different hole arrays was fabricated and the clear colorful image down to a scale of 1 μm (letter "G") was demonstrated in Figure 1(e).

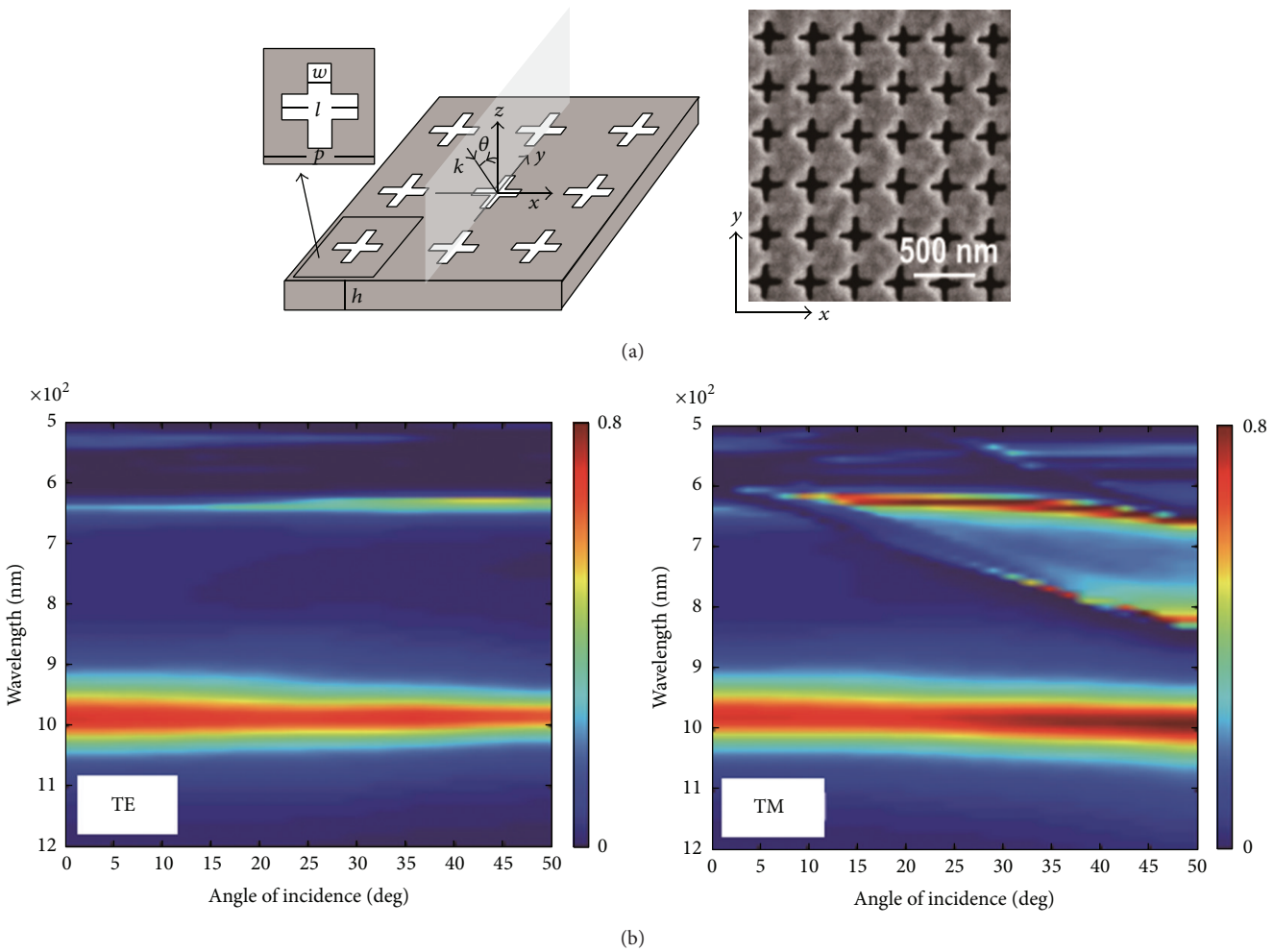

Figure 3: Angle robust metallic hole array color filter. (a) Schematic and SEM image of a cross-shape nanohole array. (b) Spectra of both polarizations for different incident angles [28].

Tunability of the structural color based on nanohole array has also been demonstrated by tuning the dielectric environment around the array [27]. As illustrated in Figure 2, the metallic hole array is patterned on top of a suspended silicon layer in a silicon-on-insulator (SOI) wafer, which is capped by a indium-tin-oxide (ITO) covered glass plate with a small gap. The hole array can be switched into contact with the glass plate by electrostatic actuation, resulting in a modified SPR due to the refractive index difference between air and glass. The substantial difference in the reflection spectra can be seen between two states as shown in Figure 2(d), which induces the variation of color.

For some applications such as image sensors and display, angular insensitivity is generally preferred. However, the filtering color of the metallic hole array varies with the incident angle as predicted in (1). When the metallic hole arrays are integrated in the imager or display to replace the pigment color filters, the issue of angle dependent color filtering should be addressed. A lot of cross-shape hole arrays show the most promising performance. In Figure 3, the cross-hole array shows excellent angle independent filtering up to 50° for both polarizations in the near infrared region [28]. The transmission peak is attributed to the excitation of localized surface plasmon resonance (LSPR) within the apertures, which is determined by the hole shape rather than the coupling between the holes for SPR in circular hole array. We scaled down the cross dimensions and optimized the transmission filtering performance for the visible band. The results are shown in Figure 4, where we can see that the transmission peaks have no obvious shift for the incident angle up to 50°. The red, green, and blue passband are clearly demonstrated.

For a more complex structure consisting of nanohole-nanodisk pair array as shown in Figure 5, there exists LSPR in the gap between nanohole and nanodisk, which induces coupling absorption of incident light due to the excitation of LSPR [29]. As a result, the LSPR dip in the reflection spectra causes a reflective color. As the LSPR effect is confined into a nanoscale, the resolution of the color image by this method could achieve 10^5 dpi, which is 100 times the state-of-the-art imaging technique. A similar dual layer structure in one dimension fabricated by interference lithography has

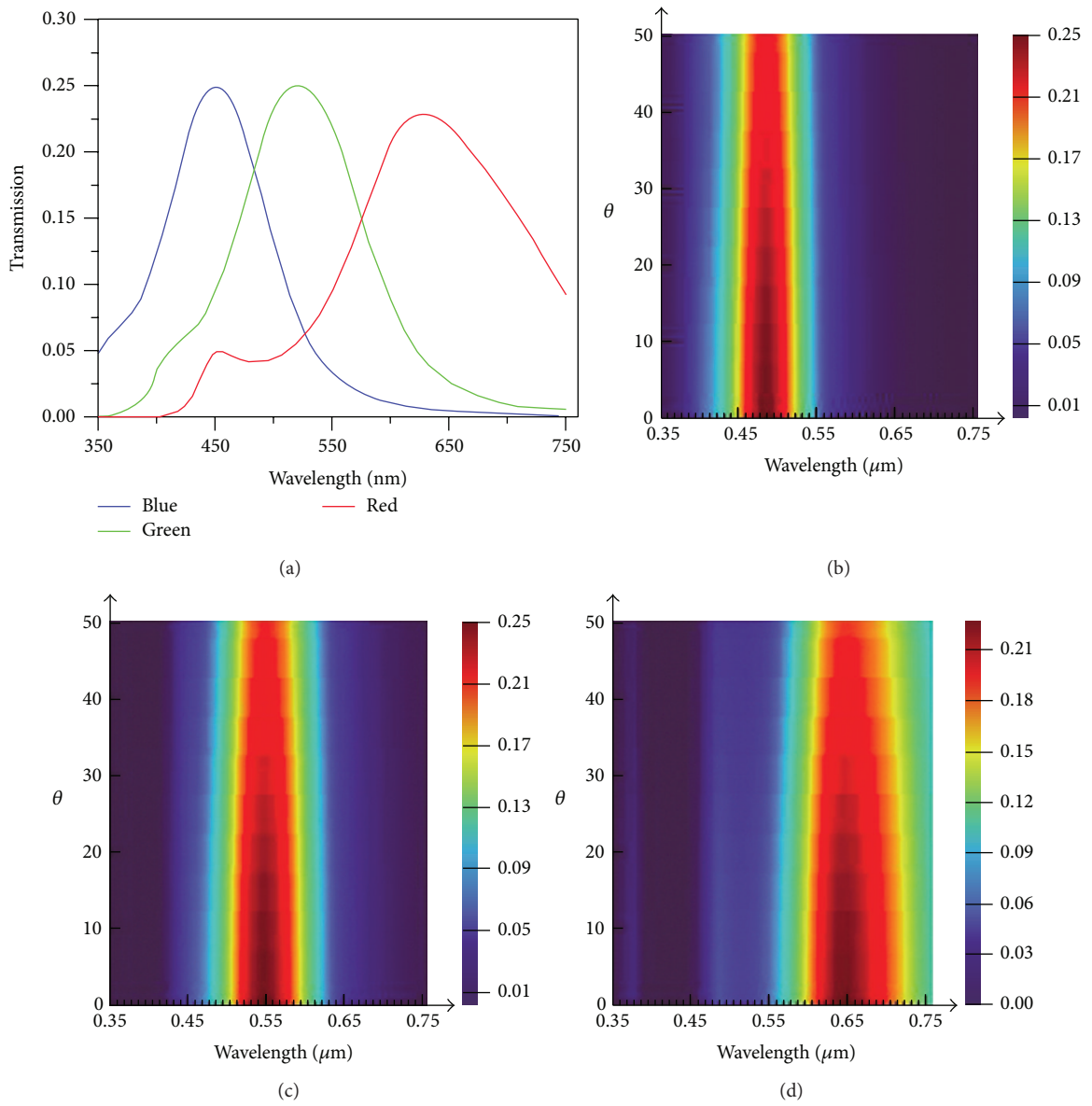

Figure 4: (a) Transmission spectra of color filters based on cross-shape nanohole array in the visible band. (b)–(d) are the transmission spectra versus incident angle θ. The geometrical parameters as defined in Figure 3(a): h = 200 nm; l = 120 nm (blue), 140 nm (green), and 180 nm (red); w = 48 nm (blue), 50 nm (green), and 40 nm (red); p = 150 nm (blue), 180 nm (green), and 230 nm (red).

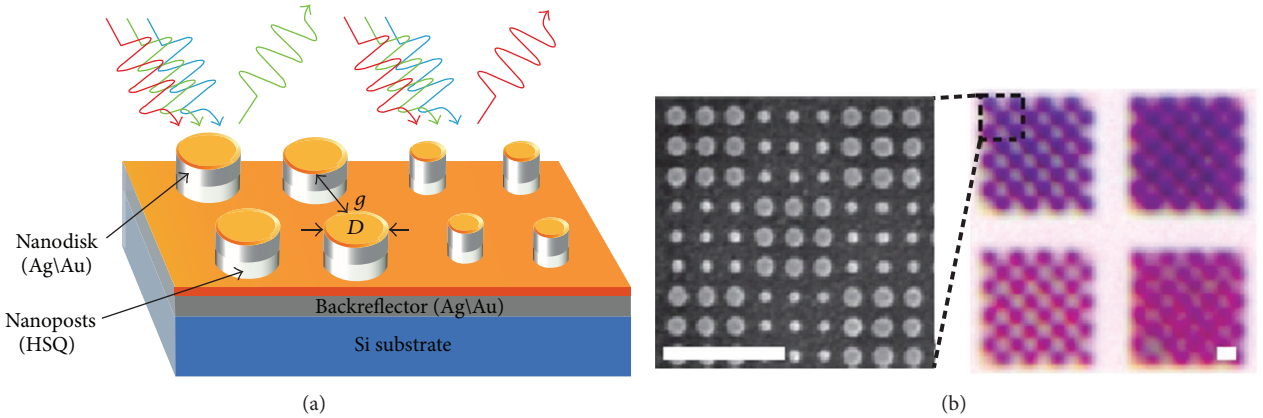

Figure 5: Nanohole-nanodisk pair array reflective color filters and the images in microscope reflection mode. Scale bar is 500 nm [29].

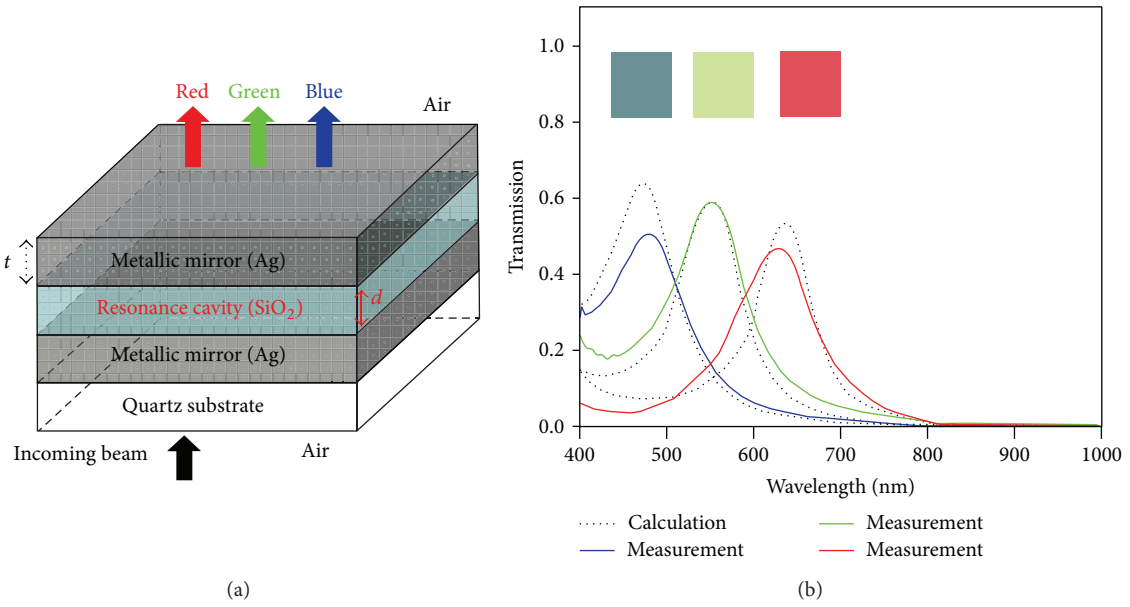

FIGURE 6: (a) Schematic of an etalon color filter. (b) Calculated and measured transmission spectra [36].

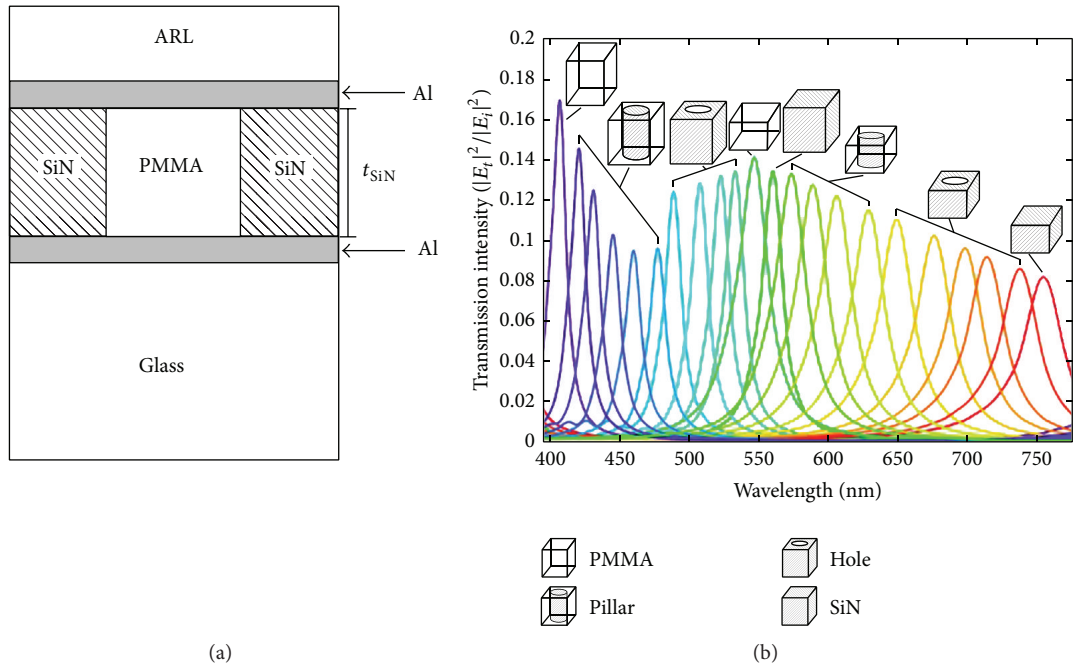

FIGURE 7: (a) Schematic and (b) simulated transmission spectra of modified etalon color filters [39].

also been demonstrated showing both color filtering and polarization functions [30]. In addition, when the bottom hole array in Figure 5 becomes a continuous metal film, the gap plasmon resonance still exists and demonstrates color filtering [31–33].

2.2. Metal-Insulator-Metal (MIM) Resonator Color Filters. Interference effect can also be used for color selection. For example, the Fabry-Pérot (FP) resonance resulting from the interference of the multiple reflected waves is normally used to determine the lasing wavelength in the laser design, where only the light at the resonance wavelength can be emitted from the cavity. A MIM structure with the semitransparent metal layer as reflective mirrors is such a configuration supporting the FP resonance [34–38]. When the thickness of the insulator layer goes down to hundreds of nanometers, the FP resonances fall into the visible region. The resonance wavelength λ can be obtained by

$$\lambda = 2n_{\text{eff}} \cdot d, \tag{2}$$

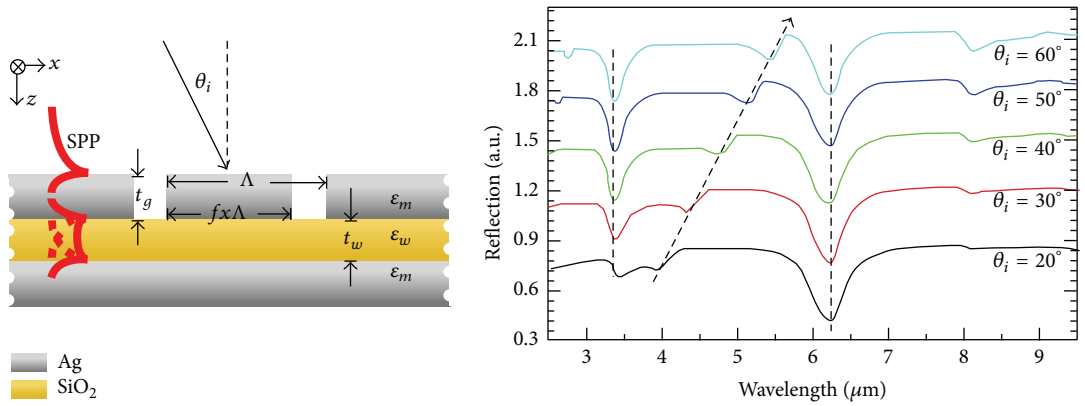

(a) (b)

FIGURE 8: (a) Schematic of MIM reflective color filters and (b) simulated reflection spectra versus incident angle [40].

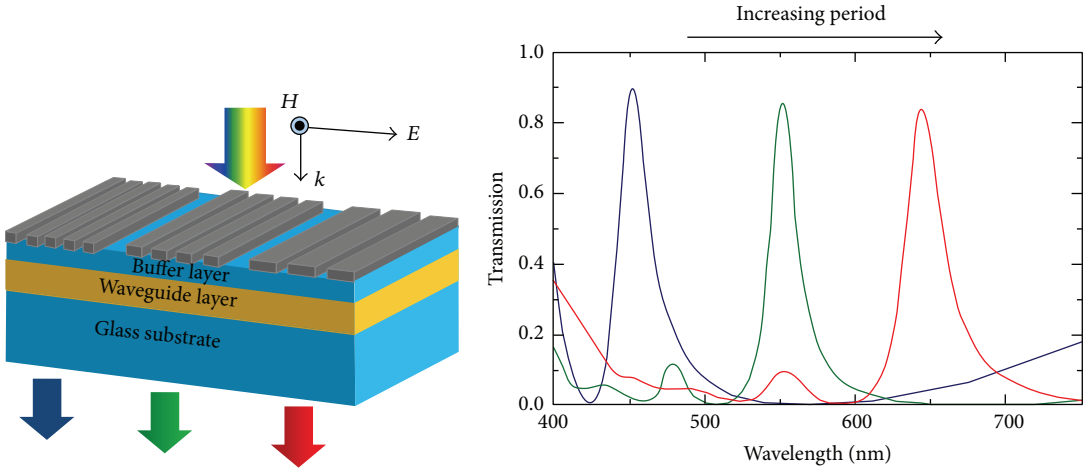

(a) (b)

FIGURE 9: (a) Schematic of a transmissive GMR color filter. (b) Simulated transmission spectra [51].

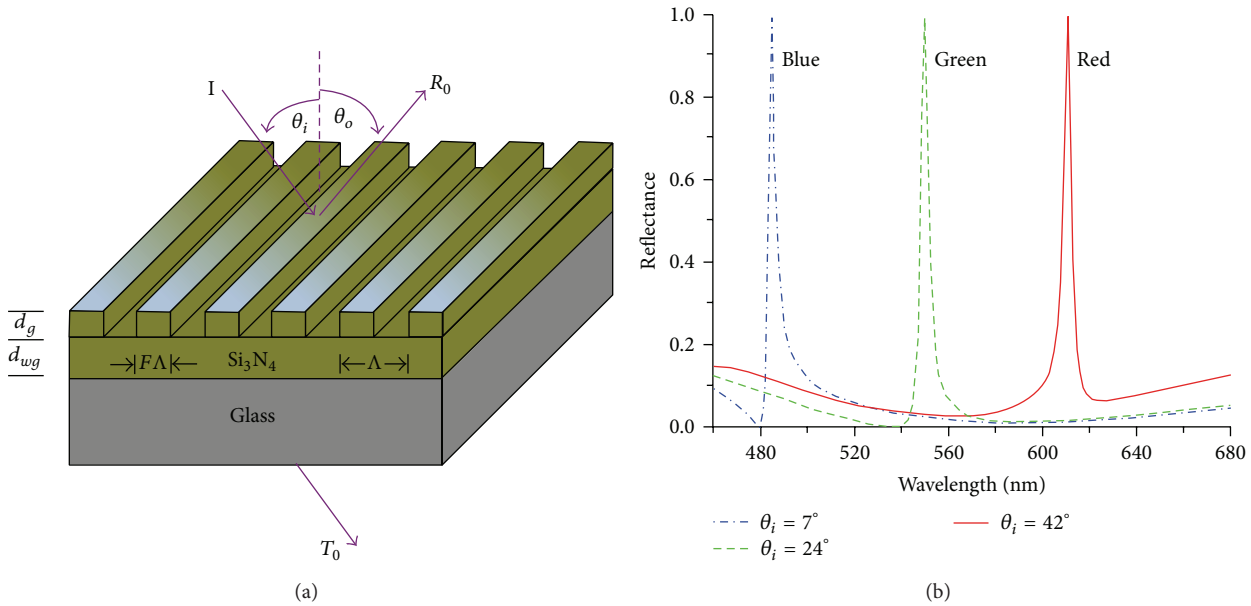

(a) (b)

FIGURE 10: (a) Schematic of a reflective GMR color filter. (b) Calculated spectral response of the tunable color filter [57].

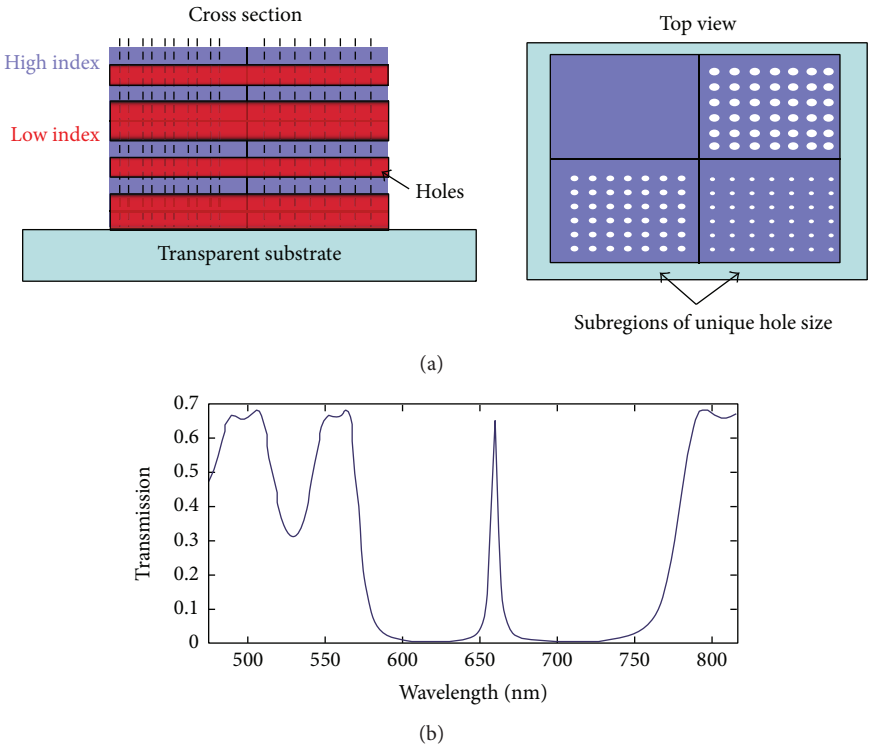

FIGURE 11: (a) Schematic of PhC color filter. (b) Transmission spectrum [62].

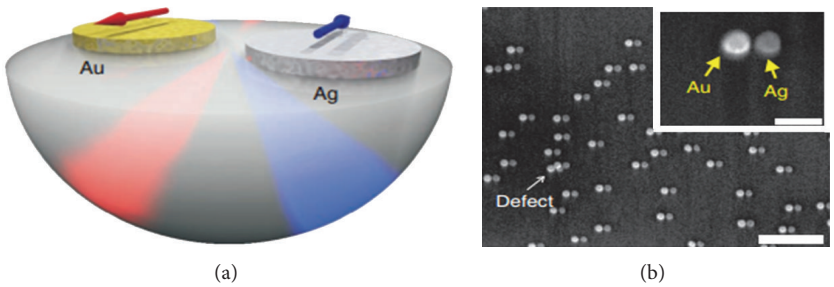

FIGURE 12: Au-Ag disk pair color routing. (a) Schematic and (b) SEM image of the fabricated sample [66].

where n_{eff} is the effective refractive index of the cavity mode and d is the cavity length.

Figure 6 shows such an etalon color filter where a Ag-SiO_2-Ag stack is used to select the transmitted wavelength [36]. Both the simulation and the measured spectra show well-defined red, green, and blue passband. A thin film of silver at 25 nm is used to ensure a reasonable transmittance and provide a mirror reflection. Because the transmission peak at the FP resonance is determined by the cavity length, different color filters need different insulator thickness, which results in multiple-step patterning if various etalon color filters are integrated. To solve this issue, we investigated a modified etalon color filter, in which the top metal mirror and the insulator layer were etched into subwavelength holes and filled with PMMA [39]. Because the hole size is smaller than the light wavelength, it can be treated as an effective material. Varying the hole size, we can change the effective refractive index of the whole stack and therefore tune the FP resonance. The schematic of this modified etalon color filter is shown in Figure 7(a) and the simulated transmission spectra are shown in Figure 7(b). By varying the hole size, the transmissive colors covering the whole visible band are achieved for only four different insulator thicknesses. Furthermore, the FWHM around 30 nm is much smaller than the hole array color filters, which has potential application in spectral imaging. Reflective color filters based on MIM structure have also been demonstrated [40, 41]. A Ag-SiO_2-Ag structure supports LSPR resulting in angle robust color filtering as shown in Figure 8 [40], which is different from FP cavity resonance. The MIM structure can also be used to tune the guided mode dispersion and construct a plasmonic lens [42–44].

2.3. Guided-Mode-Resonance (GMR) Color Filters. Diffraction is an important dispersive phenomenon, which has been widely used, for example, the dispersive gratings in

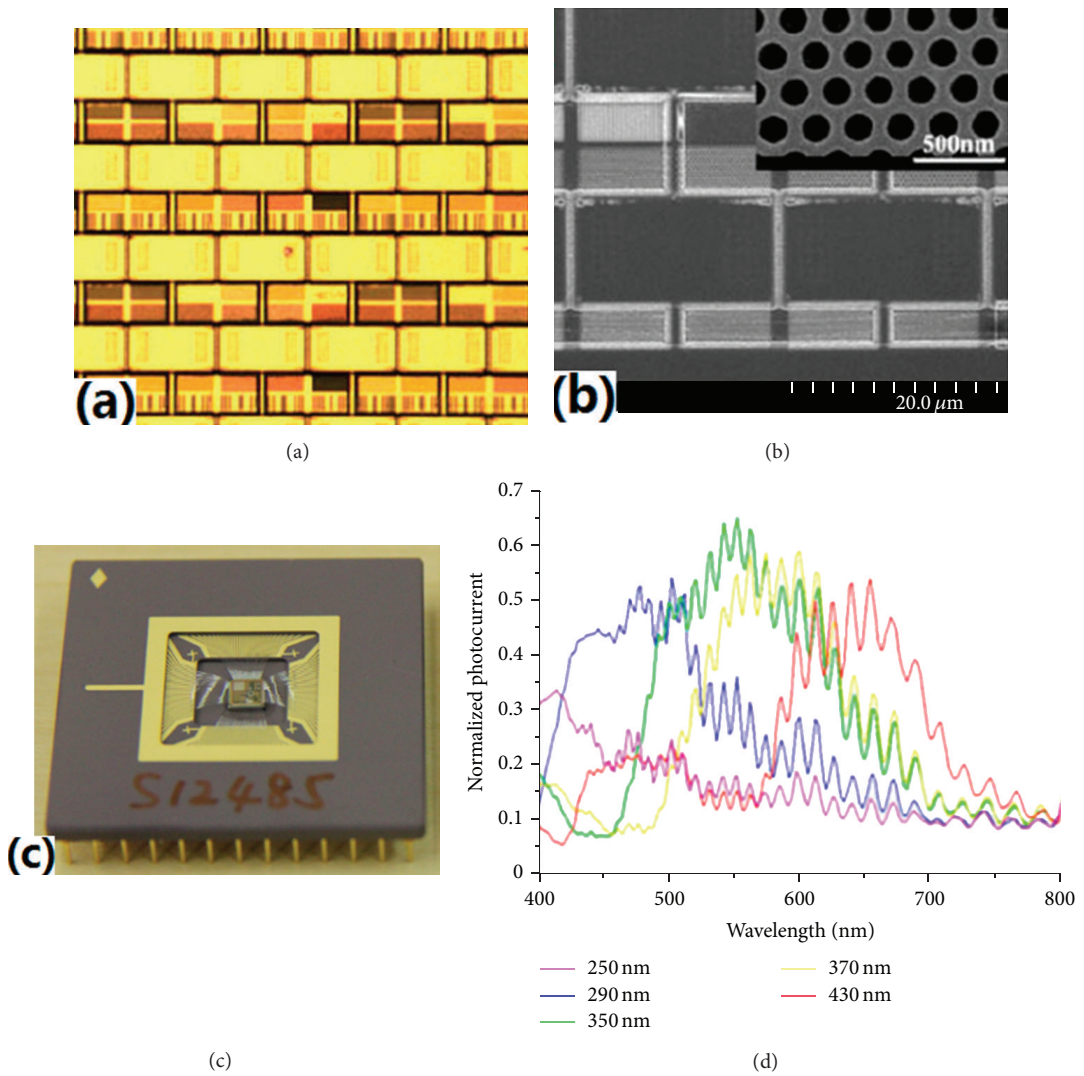

FIGURE 13: Surface plasmon enhanced CIS. (a) Microscope image and (b) SEM image of the patterned pixel array. (c) Microscope image of the packaged CIS. (d) The measured photocurrent from different pixels [18].

spectral measurement. The diffraction angle θ depends on the wavelength λ and the grating period p by the Bragg law:

$$p \cdot \sin\theta = \frac{m \cdot \lambda}{2}, \tag{3}$$

where m is an integer that stands for the diffraction order. Light at different wavelengths can be diffracted to different directions determined by the grating period. When the diffraction gratings are brought into contact with a waveguide, the diffracted light can be coupled with a guided mode when the wavevector matching condition is matched:

$$\beta = \frac{2\pi}{p}, \tag{4}$$

where β is the propagation constant of the guided mode. The coupling results in GMR that can be used for color filtering [45–58]. Kaplan et al. proposed a GMR transmissive color filter with a buffer layer between the metallic gratings and the waveguide layer [51], where the buffer layer reduces the overlap of the guided mode and the metal to reduce the absorption loss. As a result, the transmission is much higher than other structural filters and the passband is very narrow as shown in Figure 9. GMR effect can also be used in reflective color filters, where dielectric gratings are usually used to provide the coupling between the reflected diffraction and the waveguide mode. Uddin and Magnusson demonstrated such a reflective color filter by fabricating Si_3N_4 gratings on a glass slide as shown in Figure 10 [57]. However, this structure is very sensitive to the incident angle due to the diffraction effect. The reflected light changes from blue to red when the viewing angle moves from 7° to 42°.

2.4. Photonic Crystal (PhC) Color Filters. PhC is a structure with subwavelength periodic refractive index variation, which has been applied to optical fiber [59], laser [60], microwave antenna [61], color filter [62], and so forth. As

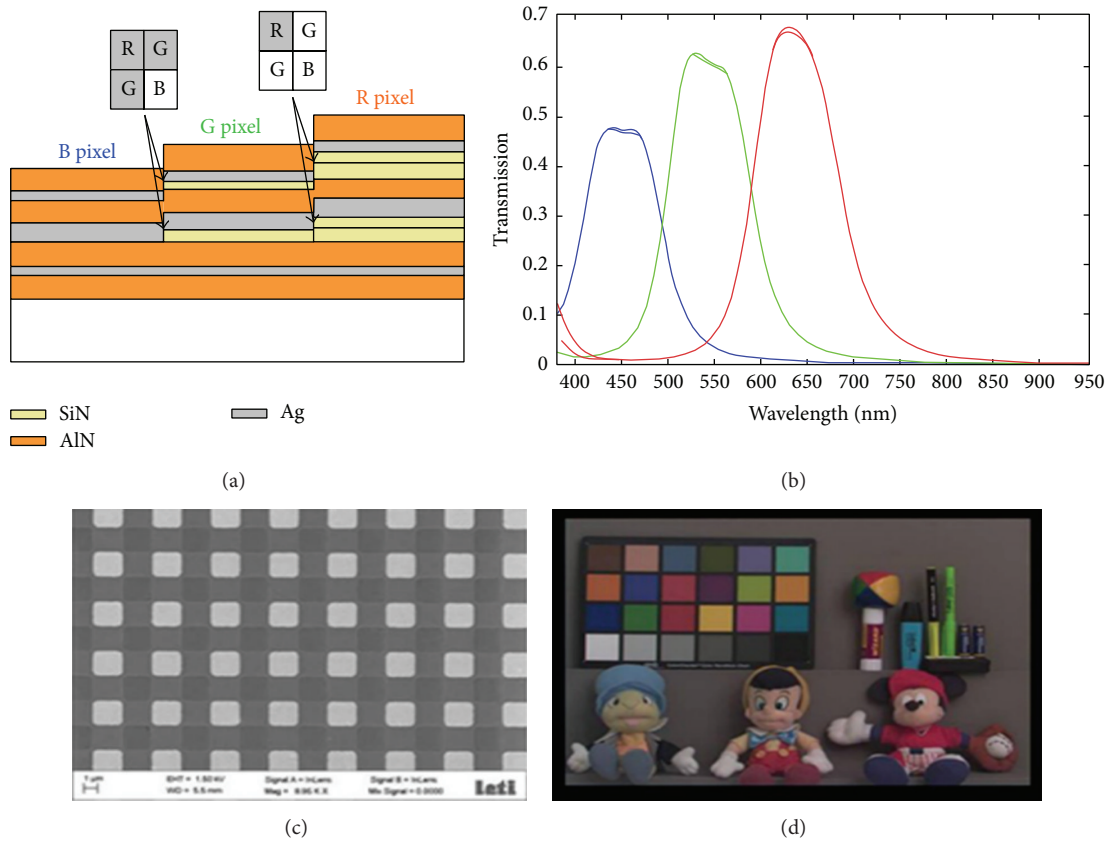

FIGURE 14: CIS using MIM color filters. (a) Schematic of the MIM color filters. (b) Simulated spectra. (c) SEM image of the pixel array. (d) A color image recorded by this CIS [38].

the electron energy band in solid state physics, photonic band can be engineered by modifying the structure of PhC [63–65]. One-dimensional PhC is a perfect reflector with the lowpass band. If a defect layer is introduced, a defect energy level appears in the bandgap, that is, a passband [51, 56, 57]. Figure 11 shows a transmission PhC color filter [62]. We can see that a 70% transmission peak with a very narrow bandwidth shows in the energy band of PhC. With optimization, if a single transmission peak can be achieved in the visible band, we can have a very high color purity and brightness. By etching holes with different sizes as the etalon color filters above, the passband can also be tuned.

2.5. Color Routing by Scattering. Light scattering usually occurs when light spreads through inhomogeneous medium. Part of light deviates from original direction with the deviation angle depending on the wavelength. Scattering from both metallic and dielectric scatters shows dispersive behavior [66–68]. Recently, Küll proposed a gold-silver disk pair for color routing as shown in Figure 12, where the phase accumulation through material-dependent plasmon resonances induces fantastic optical properties, that is, scattering red and blue light in opposite directions. This color routing device is as small as $\lambda^3/100$ [66]. It is very attractive for high-resolution imaging, but the light scattering efficiency is quite low. A dielectric light deflector of a SiN_x bar as small as 280 nm was reported recently for color routing in a CMOS image sensor by Panasonic [68]. The large refractive index contrast between the deflector and the surrounding material induces a near-field deflection with a strong dispersion (Figure 15). One of the most important advantages of the scattering color routing is that almost all energy in the spectral band is used for colorful imaging. In contrast, there is reflection/transmission loss for the transmissive/reflective color filters based on nanohole array, GMR, and MIM techniques.

3. Applications

3.1. CMOS Image Sensors (CIS). CIS are the leading mass-market technology for digital imaging. Conventional color filtering technique for CIS uses pigment or dye filters [69]. However, these polymer based color filters cannot sustain heat and radiation. Furthermore, each color filter for red, green, and blue on the pixel arrays must be fabricated step by step with accurate alignment. Therefore, structural color filters, whose performance is based on the stable metal or dielectric subwavelength structures, are very attractive. Various color filters can be fabricated using the same material and in a single lithography step.

As shown in Figure 13, we fabricated metallic nanohole array color filters on top of the pixel array of CIS and

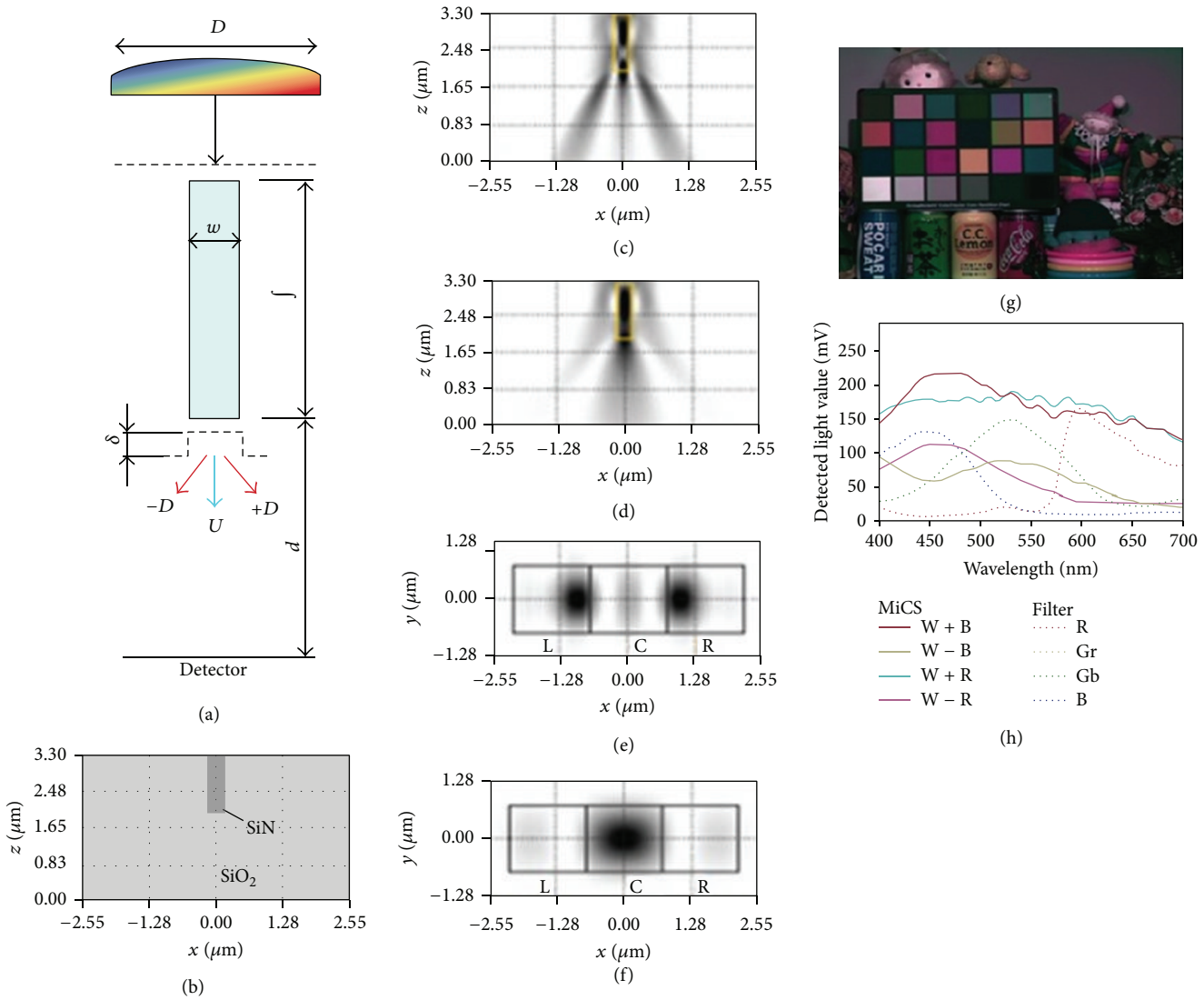

FIGURE 15: CIS based on scattering color. Left: SiN_x bar deflector; right: detected light signals from different pixels and the recorded image [68].

demonstrate the potential imaging function by measuring the photocurrent response from separated pixels [18]. The results agree with the design quite well and the distinct color filtering is achieved. For the pixels with hole arrays with period of 250 nm–430 nm, the photocurrents show intensity peaks of 450 nm–650 nm. Although the metallic hole array was fabricated by EBL directly on top of the CIS chip, the full CMOS integration of these color filters in the metal interconnect layers can be readily achieved by the state-of-the-art CMOS technologies. CEA and STM Electronics demonstrated this idea using the MIM resonator color filters [38]. And a 300 M-pixel CIS with full functions was demonstrated as seen in Figure 14. Because the MIM resonator color filter has to use space layers with different thicknesses for different colors, multistep lithography process was used. In 2013, Panasonic Ltd. presented a CIS with a pixel size as small as 1.43 μm × 1.43 μm^2, in which a 280 nm wide SiN bar was used as the light scatter to direct incident light as shown in Figure 15 [68]. As discussed in the previous section, the scattering technique for color routing suffers very little light reflection/transmission loss. 1.85 times improvement of the amount of light received by each pixel was achieved.

3.2. Colorful Solar Cells. As introduced in Section 2, sub-wavelength metallic gratings can reflect light in different colors. When these gratings are integrated in solar cells, the transmitted light is absorbed in the active layer and converted into charge, but the reflected light shows color. By attaching these colorful solar cells on the walls and roofs of the buildings, they provide both decoration and power. It is also photovoltaic color filters, which can be used in self-powering electric display device. Park et al. demonstrated this idea in an organic solar cell [70]. As shown in Figure 16, the P3HT:PCBM photoactive layer is sandwiched by an Au nanograting layer and a continuous

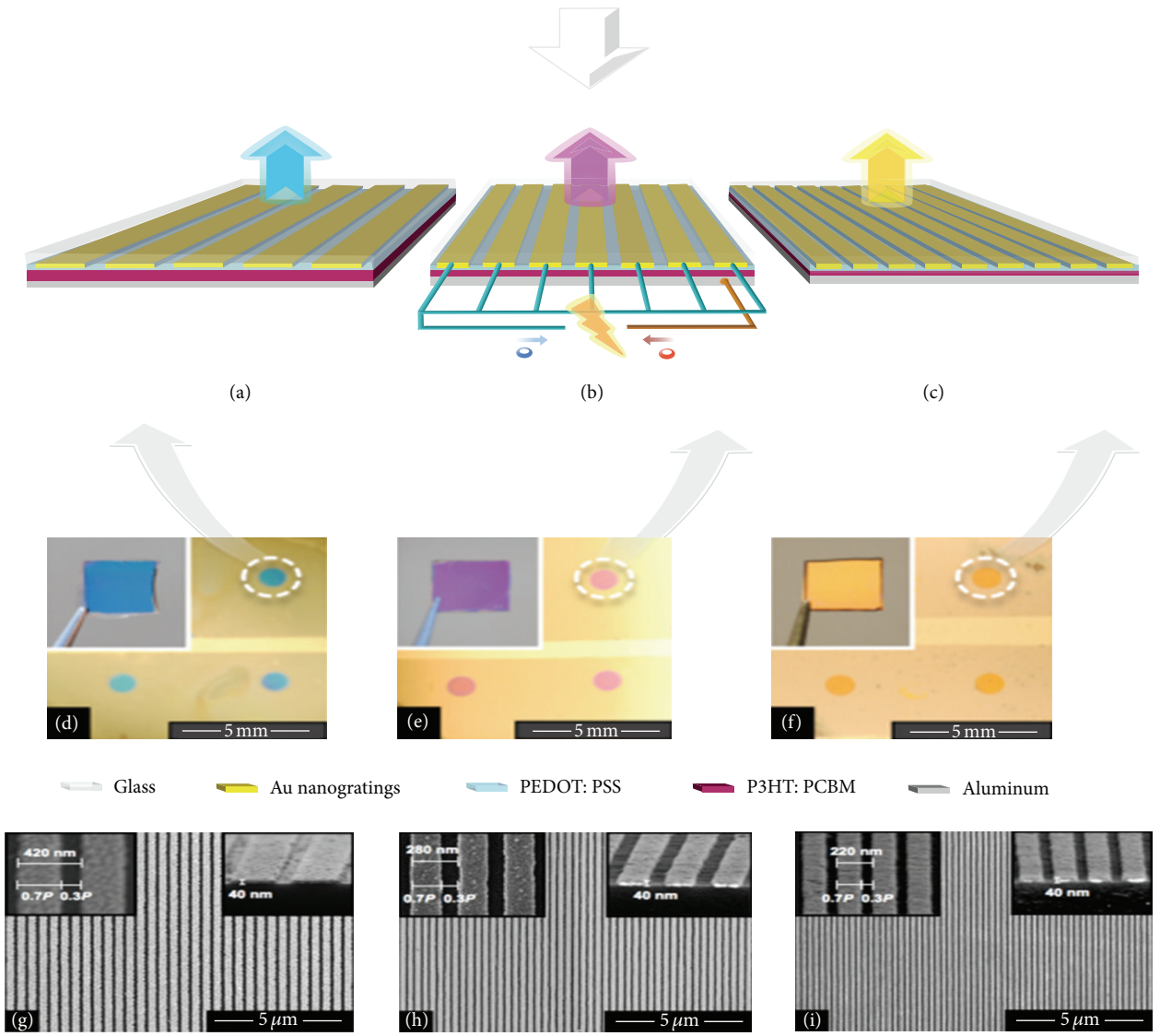

Figure 16: Colorful solar cells with the metallic gratings integrated with the organic active material [70].

Al film. The Au nanogratings are used as semitransparent electrodes for the solar cells and reflect light in different colors. Meanwhile, spectral engineering of light transmission for the transparent solar cells (TSCs) allows us to achieve more aesthetically pleasing indoor lighting with the multicolored solar windows. Transmissive colorful solar cells were developed by integrating MIM resonant color filters in Figure 17(a) [71]. As shown in Figure 17(b), by tuning the relative layer thickness of the MIM stacks, narrow-band coloring can be achieved for the TSCs. Efficiency of 5% on average was obtained for the colored TSCs, but at the expense of a rather limited luminosity. Lee et al. presented an ultrathin undoped amorphous silicon/organic hybrid solar cell structure [72]. The simple diagram of the structure can be seen in Figure 18(a). To achieve color tunability, inorganic absorbing layers with 6 nm, 11 nm, and 31 nm were selected to produced blue, green, and red cells. The structures show that the transmissive spectra have great angle insensitivity in Figures 18(b)–18(g). Although, monochromatic coloring and near unity internal quantum efficiency were obtained, their efficiencies were significantly undermined by the poor light-harvesting capacity for such ultrathin absorbing layers. Actually, the metallic gratings can be used to tune the absorption spectrum of solar cell and achieve a significant improvement of the absorption due to effects such as LSPR, GMR, and FP resonance [73].

3.3. Colorful OLED Display. Although colorful OLEDs can be obtained by using different electroluminescence (EL) materials, the intrinsic emission spectra of EL materials are not narrow enough for high purity colorful display. Furthermore, different EL materials have to be used in display to generate the full color, which needs multiple lithography process like the pigment color filters in CIS. The combination of white OLED and color filters has lower cost and higher

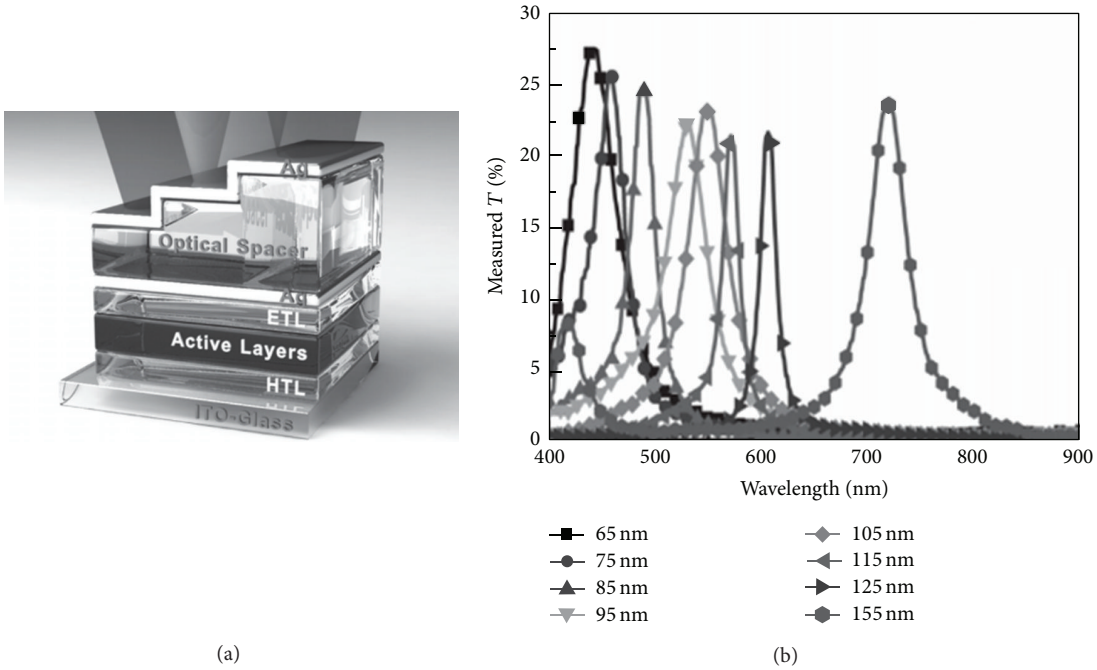

Figure 17: (a) Device architecture of MIM transmissive solar cell. (b) The measured transmissive spectra [71].

yield. In order to improve the purity of the color, many researchers have engaged in OLED with different types of color filters. For example, both one dimensional metal slits and two dimensional nanoholes have been theoretically and experimentally demonstrated [74, 75]. A narrow band and high transmission can be achieved by changing the parameter of the color filters, making these types of color filters have potential advantages in OLED display. As shown in Figure 19, in the color filters, distributed Bragg reflector acts as the half mirror; IZO/ITO and SiN_x are used as the optical filler to tune the color [76]. By integrating the structures at the emitting surface of the OLED, a set of colorful OLEDs were achieved. Photograph of a display fabricated with this design clearly shows the excellent color performance.

4. Discussion

From the above, we can see that structural color filters have attracted extensive interest from both academia and industry due to advantages such as high resistance, high stability, high compactness, tunability, low loss, and functionalities. There are also issues to be addressed before the massive applications. First, high resolution, high throughput, and low cost fabrication techniques of structure colors need be developed. Because of the short wavelength of the visible light, the structural colors are usually based on sub-μm structures, which is a challenge for current microfabrication techniques. Nanoimprint and interference lithography could be an answer to this issue. Second, overall optimization of light efficiency, cross-talk, and angle insensitivity need be considered. Metallic hole array shows low transmission; GMR has strong angle dependence; scattering has a significant cross-talk; MIM and PhC also surfer angle sensitivity. Third, there are integration issues of structural color filters, for example, metal loss and compatibility with the industrial processes. Advanced fabrication technology, new photonic mechanism, and novel device design would be developed to address these issues.

5. Summary and Outlook

We review the recent development of transmissive/reflective structural color techniques including nanohole array, MIM resonator, GMR effect, photonic crystal, and light scattering. Mechanisms and performances of various structural color filters are presented, together with the integrated applications in CIS, display, solar cells, and OLEDs. The results are promising and some prototype devices have been achieved. We consider that these structural color filters still have a long way to go before extensive commercialization. The next step for the research will focus on improving the transmission/reflection efficiency, reducing the bandwidth, suppressing the angular dependence, and so forth. High throughput and low cost fabrication technologies are also required. We believe structural color filters can be more extensively applied in our life.

Conflict of Interests

The authors declare that there is no conflict of interests regarding the publication of this paper.

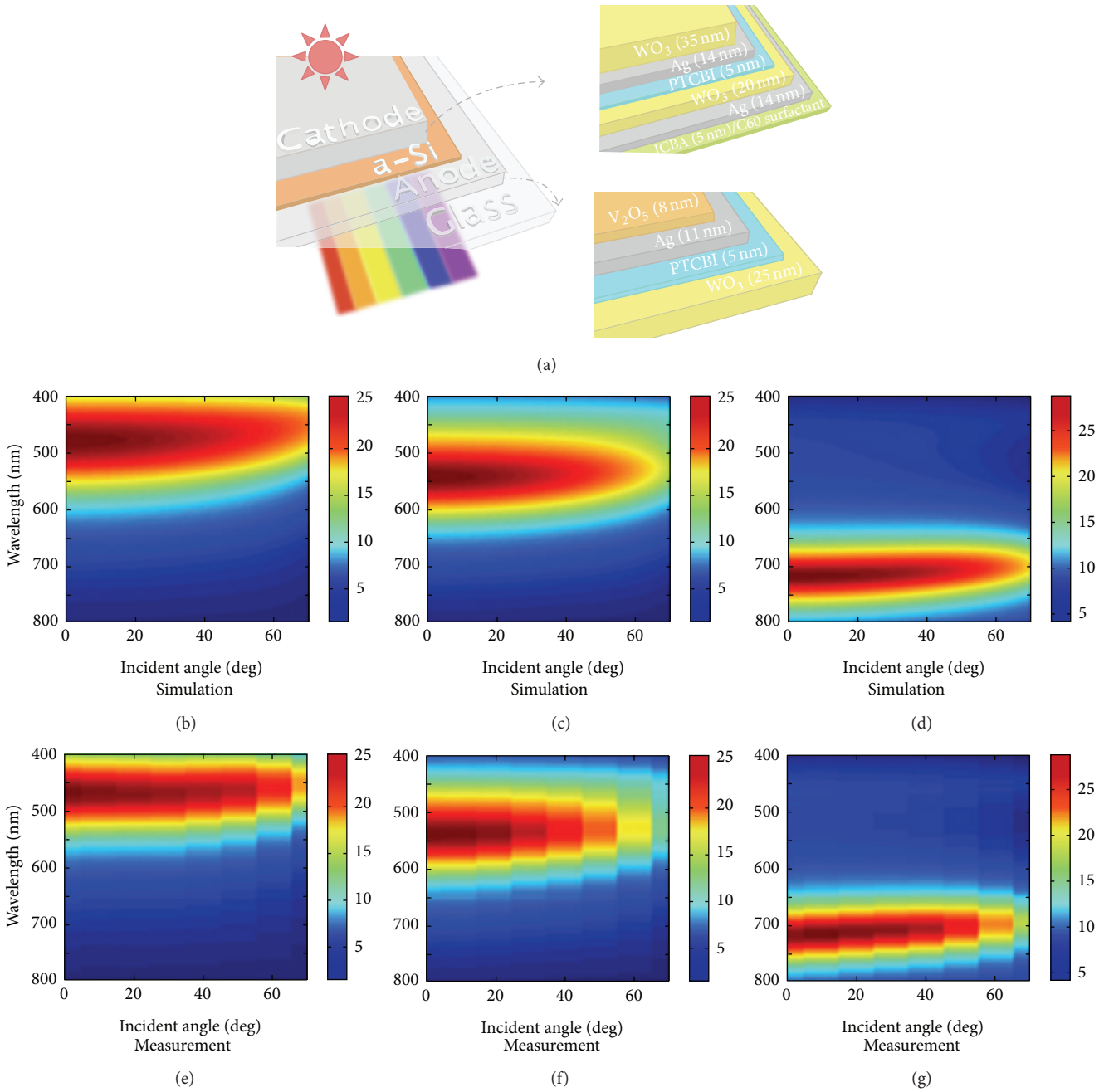

Figure 18: (a) Schematic of the angle insensitive structure. (b)–(d) and (e)–(g) are the simulated and measured relationship between incident angle and transmission [72].

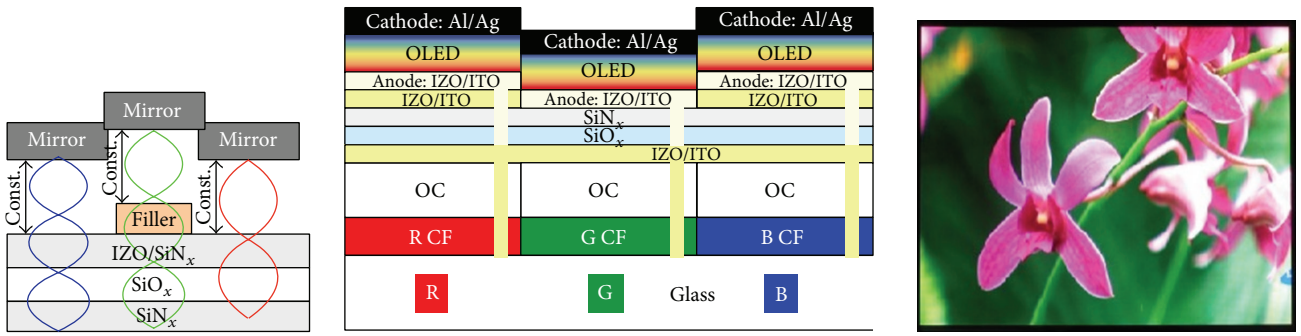

Figure 19: Microcavity embedded RGBW bottom-emitting AMOLED and the photograph of a display fabricated with the design [76].

Acknowledgments

This work is supported by Grants from the National Natural Science Foundation of China (no. 11274344), the Hundred Talents Program of the Chinese Academy of Sciences, the Scientific Research Foundation for the Returned Overseas Chinese Scholars, the State Education Ministry, and the Fundamental Research Project of Shenzhen Science and Technology Foundation (no. JC201105180781A).

References

[1] H. Koo, M. Chen, and P. Pan, "LCD-based color filter films fabricated by a pigment-based colorant photo resist inks and printing technology," *Thin Solid Films*, vol. 515, no. 3, pp. 896–901, 2006.

[2] M. C. Gather, A. Köhnen, A. Falcou, H. Becker, and K. Meerholz, "Solution-processed full-color polymer organic light-emitting diode displays fabricated by direct photolithography," *Advanced Functional Materials*, vol. 17, no. 2, pp. 191–200, 2007.

[3] T. Xu, H. Shi, Y. Wu, A. F. Kaplan, J. G. Ok, and L. J. Guo, "Structural colors: from plasmonic to carbon nanostructures," *Small*, vol. 7, no. 22, pp. 3128–3136, 2011.

[4] J. J. Cowan, "Aztec surface-relief volume diffractive structure," *Journal of the Optical Society of America A*, vol. 7, no. 8, pp. 1529–1544, 1990.

[5] T. W. Ebbesen, H. J. Lezec, H. F. Ghaemi, T. Thio, and P. A. Wolff, "Extraordinary optical transmission through sub-wavelenght hole arrays," *Nature*, vol. 391, no. 6668, pp. 667–669, 1998.

[6] H. A. Bethe, "Theory of diffraction by small holes," *Physical Review*, vol. 66, no. 7-8, pp. 163–182, 1944.

[7] H. F. Ghaemi, T. Thio, D. E. Grupp, T. W. Ebbesen, and H. J. Lezec, "Surface plasmons enhance optical transmission through subwavelength holes," *Physical Review B. Condensed Matter and Materials Physics*, vol. 58, no. 11, pp. 6779–6782, 1998.

[8] J. A. Porto, F. J. García-Vidal, and J. B. Pendry, "Transmission resonances on metallic gratings with very narrow slits," *Physical Review Letters*, vol. 83, no. 14, pp. 2845–2848, 1999.

[9] M. N. E. Popov, S. Enoch, and R. Reinisch, "Theory of light transmission through subwavelength periodic hole arrays," *Physical Review B*, vol. 62, Article ID 16100, 2000.

[10] Q. Cao and P. Lalanne, "Negative role of surface plasmons in the transmission of metallic gratings with very narrow slits," *Physical Review Letters*, vol. 88, no. 5, Article ID 057403, 2002.

[11] K. Walls, Q. Chen, S. Collins, D. R. S. Cumming, and T. D. Drysdale, "Automated design, fabrication, and characterization of color matching plasmonic filters," *IEEE Photonics Technology Letters*, vol. 24, no. 7, pp. 602–604, 2012.

[12] H. Lee, Y. Yoon, S. Lee, S. Kim, and K. Lee, "Color filter based on a subwavelength patterned metal grating," *Optics Express*, vol. 15, no. 23, pp. 15457–15463, 2007.

[13] W. Li and S. Y. Chou, "Solar-blind deep-UV band-pass filter (250–350 nm) consisting of a metal nano-grid fabricated by nanoimprint lithography," *Optics Express*, vol. 18, no. 2, pp. 931–937, 2010.

[14] Q. Chen and D. R. S. Cumming, "High transmission and low color cross-talk plasmonic color filters using triangular-lattice hole arrays in aluminum films," *Optics Express*, vol. 18, no. 13, pp. 14056–14062, 2010.

[15] D. Inoue, A. Miura, T. Nomura et al., "Polarization independent visible color filter comprising an aluminum film with surface-plasmon enhanced transmission through a subwavelength array of holes," *Applied Physics Letters*, vol. 98, no. 9, Article ID 093113, 2011.

[16] G. Si, Y. Zhao, H. Liu et al., "Annular aperture array based color filter," *Applied Physics Letters*, vol. 99, no. 3, Article ID 033105, 2011.

[17] Q. Chen, D. Chitnis, K. Walls, T. D. Drysdale, S. Collins, and D. R. S. Cumming, "CMOS photodetectors integrated with plasmonic color filters," *IEEE Photonics Technology Letters*, vol. 24, no. 3, pp. 197–199, 2012.

[18] Q. Chen, D. Das, D. Chitnis et al., "A CMOS image sensor integrated with plasmonic colour filters," *Plasmonics*, vol. 7, no. 4, pp. 695–699, 2012.

[19] F. Przybilla, A. Degiron, C. Genet et al., "Efficiency and finite size effects in enhanced transmission through subwavelength apertures," *Optics Express*, vol. 16, no. 13, pp. 9571–9579, 2008.

[20] S. Yokogawa, S. P. Burgos, and H. A. Atwater, "Plasmonic color filters for CMOS image sensor applications," *Nano Letters*, vol. 12, no. 8, pp. 4349–4354, 2012.

[21] S. P. Burgos, S. Yokogawa, and H. A. Atwater, "Color imaging via nearest neighbor hole coupling in plasmonic color filters integrated onto a complementary metal-oxide semiconductor image sensor," *Acs Nano*, vol. 7, no. 11, pp. 10038–10047, 2013.

[22] D. van Labeke, D. Gérard, B. Guizal, F. I. Baida, and F. Li, "An angle-independent frequency selective surface in the optical range," *Optics Express*, vol. 14, no. 25, pp. 11945–11951, 2006.

[23] S. Y. Chou, P. R. Krauss, and P. J. Renstrom, "Nanoimprint lithography," *Journal of Vacuum Science and Technology B: Microelectronics and Nanometer Structures*, vol. 14, no. 6, pp. 4129–4133, 1996.

[24] Q. Chen, G. Hubbard, P. A. Shields et al., "Broadband moth-eye antireflection coatings fabricated by low-cost nanoimprinting," *Applied Physics Letters*, vol. 94, no. 26, Article ID 263118, 2009.

[25] G. Hubbard, S. J. Abbott, Q. Chen et al., "Wafer-scale transfer of nanoimprinted patterns into silicon substrates," *Physica E: Low-Dimensional Systems and Nanostructures*, vol. 41, no. 6, pp. 1118–1121, 2009.

[26] Q. Chen, C. Martin, and D. R. S. Cumming, "Transfer printing of nanoplasmonic devices onto flexible polymer substrates from a rigid stamp," *Plasmonics*, vol. 7, no. 4, pp. 755–761, 2012.

[27] J. L. Skinner, A. A. Talin, and D. A. Horsley, "A MEMS light modulator based on diffractive nanohole gratings," *Optics Express*, vol. 16, no. 6, pp. 3701–3711, 2008.

[28] L. Lin and A. Roberts, "Angle-robust resonances in cross-shaped aperture arrays," *Applied Physics Letters*, vol. 97, no. 6, Article ID 061109, 2010.

[29] K. Kumar, H. Duan, R. S. Hegde, S. C. W. Koh, J. N. Wei, and J. K. W. Yang, "Printing colour at the optical diffraction limit," *Nature Nanotechnology*, vol. 7, no. 9, pp. 557–561, 2012.

[30] Z. Ye, J. Zheng, S. Sun, L. Guo, and H. D. Shieh, "Compact transreflective color filters and polarizers by bilayer metallic nanowire gratings on flexible substrates," *IEEE Journal on Selected Topics in Quantum Electronics*, vol. 19, no. 3, pp. 4800205–4800209, 2013.

[31] A. S. Roberts, A. Pors, O. Albrektsen, and S. I. Bozhevolnyi, "Subwavelength plasmonic color printing protected for ambient use," *Nano Letters*, vol. 14, no. 2, pp. 783–787, 2014.

[32] S. Song, Q. Chen, L. Jin, and F. Sun, "Great light absorption enhancement in a graphene photodetector integrated with a

metamaterial perfect absorber," *Nanoscale*, vol. 5, no. 20, pp. 9615–9619, 2013.

[33] Q. Chen, F. Sun, and S. Song, "Subcell misalignment in vertically cascaded metamaterial absorbers," *Optics Express*, vol. 21, no. 13, pp. 15896–15903, 2013.

[34] W. Cai, U. K. Chettiar, H. Yuan et al., "Metamagnetics with rainbow colors," *Optics Express*, vol. 15, no. 6, pp. 3333–3341, 2007.

[35] Z. Wu, D. Lee, M. F. Rubner, and R. E. Cohen, "Structural color in porous, superhydrophilic, and self-cleaning SiO_2/TiO_2 bragg stacks," *Small*, vol. 3, no. 8, pp. 1445–1451, 2007.

[36] Y.-T. Yoon and S.-S. Lee, "Transmission type color filter incorporating a silver film based etalon," *Optics Express*, vol. 18, no. 5, pp. 5344–5349, 2010.

[37] T. Xu, Y. Wu, X. Luo, and L. J. Guo, "Plasmonic nanoresonators for high-resolution colour filtering and spectral imaging," *Nature Communications*, vol. 1, pp. 59–63, 2010.

[38] L. Frey, P. Parrein, J. Raby et al., "Color filters including infrared cut-off integrated on CMOS image sensor," *Optics Express*, vol. 19, no. 14, pp. 13073–13080, 2011.

[39] K. Walls, Q. Chen, J. Grant, S. Collins, D. R. S. Cumming, and T. D. Drysdale, "Narrowband multispectral filter set for visible band," *Optics Express*, vol. 20, no. 20, pp. 21917–21923, 2012.

[40] C. M. Wang, Y. C. Chang, M. W. Tsai et al., "Angle-independent infrared filter assisted by localized surface plasmon polariton," *IEEE Photonics Technology Letters*, vol. 20, no. 13, pp. 1103–1105, 2008.

[41] A. F. Kaplan, T. Xu, Y. Wu, and L. J. Guo, "Multilayer pattern transfer for plasmonic color filter applications," *Journal of Vacuum Science and Technology B: Microelectronics and Nanometer Structures*, vol. 28, no. 6, Article ID C6O60, 2010.

[42] Q. Chen and D. R. S. Cumming, "Visible light focusing demonstrated by plasmonic lenses based on nano-slits in an aluminum film," *Optics Express*, vol. 18, no. 14, pp. 14762–14767, 2010.

[43] Q. Chen, "Effect of the number of zones in a one-dimensional plasmonic zone plate lens: simulation and experiment," *Plasmonics*, vol. 6, no. 1, pp. 75–82, 2011.

[44] Q. Chen, "A Novel Plasmonic Zone Plate Lens Based on Nano-Slits with Refractive Index Modulation," *Plasmonics*, vol. 6, no. 2, pp. 381–385, 2011.

[45] W. Nakagawa, P. Sun, C. Chen, and Y. Fainman, "Wide-field-of-view narrow-band spectral filters based on photonic crystal nanocavities," *Optics Letters*, vol. 27, no. 3, pp. 191–193, 2002.

[46] A. Mehta, R. C. Rumpf, Z. Roth, and E. G. Johnson, "Nanofabrication of a space-variant optical transmission filter," *Optics Letters*, vol. 31, no. 19, pp. 2903–2905, 2006.

[47] S. S. Wang and R. Magnusson, "Theory and applications of guide-mode resonance filters," *Applied Optics*, vol. 32, no. 14, pp. 2606–2613, 1993.

[48] Y. Kanamori, M. Shimono, and K. Hane, "Fabrication of transmission color filters using silicon subwavelength gratings on quartz substrates," *IEEE Photonics Technology Letters*, vol. 18, no. 20, pp. 2126–2128, 2006.

[49] Y. T. Yoon, H. S. Lee, S. S. Lee, S. H. Kim, J. D. Park, and K. Lee, "Color filter incorporating a subwavelength patterned grating in poly silicon," *Optics Express*, vol. 16, no. 4, pp. 2374–2380, 2008.

[50] B. Luk'Yanchuk, N. I. Zheludev, S. A. Maier et al., "The Fano resonance in plasmonic nanostructures and metamaterials," *Nature Materials*, vol. 9, no. 9, pp. 707–715, 2010.

[51] A. F. Kaplan, T. Xu, and L. Jay Guo, "High efficiency resonance-based spectrum filters with tunable transmission bandwidth fabricated using nanoimprint lithography," *Applied Physics Letters*, vol. 99, no. 14, Article ID 143111, 2011.

[52] K. Kintaka, T. Majima, J. Inoue, K. Hatanaka, J. Nishii, and S. Ura, "Cavity-resonator-integrated guided-mode resonance filter for aperture miniaturization," *Optics Express*, vol. 20, no. 2, pp. 1444–1449, 2012.

[53] I. R. Mckerracher, L. Fu, H. H. Tan, and C. Jagadish, "Integration of bandpass guided-mode resonance filters with mid-wavelength infrared photodetectors," *Journal of Physics D: Applied Physics*, vol. 46, no. 9, Article ID 095104, 2013.

[54] I. D. Block, M. Pineda, C. J. Choi, and B. T. Cunningham, "High sensitivity plastic-substrate photonic crystal biosensor," *IEEE Sensors Journal*, vol. 8, no. 9-10, pp. 1546–1547, 2008.

[55] S. S. Wang, R. Magnusson, J. S. Bagby, and M. G. Moharam, "Guided-mode resonances in planar dielectric-layer diffraction gratings," *Journal of the Optical Society of America A: Optics Image Science and Vision*, vol. 7, no. 8, pp. 1470–1474, 1990.

[56] N. Nguyen-Huu, Y.-L. Lo, and Y.-B. Chen, "Color filters featuring high transmission efficiency and broad bandwidth based on resonant waveguide-metallic grating," *Optics Communications*, vol. 284, no. 10-11, pp. 2473–2479, 2011.

[57] M. J. Uddin and R. Magnusson, "Efficient guided-mode-resonant tunable color filters," *IEEE Photonics Technology Letters*, vol. 24, no. 17, pp. 1552–1554, 2012.

[58] D. Rosenblatt, A. Sharon, and A. A. Friesem, "Resonant grating waveguide structures," *IEEE Journal of Quantum Electronics*, vol. 33, no. 11, pp. 2038–2059, 1997.

[59] J. C. Knight, "Photonic crystal fibres," *Nature*, vol. 424, no. 6950, pp. 847–851, 2003.

[60] H. Matsubara, S. Yoshimoto, H. Saito, Y. Jianglin, Y. Tanaka, and S. Noda, "GaN photonic-crystal surface-emitting laser at blue-violet wavelengths," *Science*, vol. 319, no. 5862, pp. 445–447, 2008.

[61] E. R. Brown, C. D. Parker, and E. Yablonovitch, "Radiation properties of a planar antenna on a photonic-crystal substrate," *Journal of the Optical Society of America B: Optical Physics*, vol. 10, no. 2, pp. 404–407, 1993.

[62] G. Shambat, R. Athale, G. Euliss, M. Mirotznik, E. Johnson, and V. Smolski, "Reconfigurable photonic crystal filters for multi-band optical filtering on a monolithic substrate," in *Proceedings of SPIE Nanostructured Thin Films*, vol. 7041, pp. 70410P1–70410P12, 2008.

[63] Q. Chen, M. D. Archbold, and D. W. E. Allsopp, "Design of ultrahigh-Q 1-D photonic crystal microcavities," *IEEE Journal of Quantum Electronics*, vol. 45, no. 3, pp. 233–239, 2009.

[64] Q. Chen and D. W. E. Allsopp, "Group velocity delay in coupled-cavity waveguides based on ultrahigh-Q cavities with Bragg reflectors," *Journal of Optics A: Pure and Applied Optics*, vol. 11, no. 5, Article ID 054010, 2009.

[65] Q. Chen and D. W. E. Allsopp, "One-dimensional coupled cavities photonic crystal filters with tapered Bragg mirrors," *Optics Communications*, vol. 281, no. 23, pp. 5771–5774, 2008.

[66] T. Shegai, S. Chen, V. D. Miljković, G. Zengin, P. Johansson, and M. Käll, "A bimetallic nanoantenna for directional colour routing," *Nature Communications*, vol. 2, no. 1, article 481, 2011.

[67] S. H. A. Lavasani and T. Pakizeh, "Color-switched directional ultracompact optical nanoantennas," *Journal of the Optical Society of America B: Optical Physics*, vol. 29, no. 6, pp. 1361–1366, 2012.

[68] S. Nishiwaki, T. Nakamura, M. Hiramoto, T. Fujii, and M. Suzuki, "Efficient colour splitters for high-pixel-density image sensors," *Nature Photonics*, vol. 7, no. 3, pp. 240–246, 2013.

[69] Y. Huo, C. C. Fesenmaier, and P. B. Catrysse, "Microlens performance limits in sub-2μm pixel CMOS image sensors," *Optics Express*, vol. 18, no. 6, pp. 5861–5872, 2010.

[70] H. J. Park, T. Xu, J. Y. Lee, A. Ledbetter, and L. J. Guo, "Photonic color filters integrated with organic solar cells for energy harvesting," *ACS Nano*, vol. 5, no. 9, pp. 7055–7060, 2011.

[71] Y. H. Chen, C. W. Chen, Z. Y. Huang et al., "Microcavity-embedded, colour-tuneable, transparent organic solar cells," *Advanced Materials*, vol. 26, no. 7, pp. 1129–1134, 2014.

[72] J. Y. Lee, K. T. Lee, S. Seo, and L. J. Guo, "Decorative power generating panels creating angle insensitive transmissive colors," *Scientific Reports*, vol. 4, pp. 4192–4197, 2014.

[73] L. Wen, F. Sun, and Q. Chen, "Cascading metallic gratings for broadband absorption enhancement in ultrathin plasmonic solar cells," *Applied Physics Letters*, vol. 104, no. 15, Article ID 151106, 2014.

[74] X. Hu, L. Zhan, and Y. Xia, "Color filters based on enhanced optical transmission of subwavelength-structured metallic film for multicolor organic light-emitting diode display," *Applied Optics*, vol. 47, no. 23, pp. 4275–4279, 2008.

[75] Y. Qiu, L. Zhan, X. Hu, S. Luo, and Y. Xia, "Demonstration of color filters for OLED display based on extraordinary optical transmission through periodic hole array on metallic film," *Displays*, vol. 32, no. 5, pp. 308–312, 2011.

[76] B. W. Lee, Y. I. Hwang, H. Y. Lee, C. W. Kim, and Y. G. Ju, "Micro-cavity design of RGBW AMOLED for 100% color gamut," in *Proceedings of the 2008 Sid International Symposium, Digest of Technical Papers*, vol. 39, pp. 1050–1053, Books I–III, 2008.